Cerebral Cortex February 2012;22:469–481
doi:10.1093/cercor/bhr301
Advance Access publication November 23, 2011

Abundant Occurrence of Basal Radial Glia in the Subventricular Zone of Embryonic Neocortex of a Lissencephalic Primate, the Common Marmoset *Callithrix jacchus*

Iva Kelava[1], Isabel Reillo[2], Ayako Y. Murayama[3], Alex T. Kalinka[1], Denise Stenzel[1], Pavel Tomancak[1], Fumio Matsuzaki[4], Cécile Lebrand[5], Erika Sasaki[6,7], Jens C. Schwamborn[8], Hideyuki Okano[3,9], Wieland B. Huttner[1] and Víctor Borrell[2]

[1]Max-Planck-Institute of Molecular Cell Biology and Genetics, D-01307 Dresden, Germany, [2]Developmental Neurobiology Unit, Instituto de Neurociencias, Consejo Superior de Investigaciones Científicas—Universidad Miguel Hernández, 03550 Sant Joan d'Alacant, Spain, [3]Department of Physiology, Keio University School of Medicine, Tokyo 160-8582, Japan, [4]RIKEN Center for Developmental Biology, Kobe 650-0047, Japan, [5]Department of Cellular Biology and Morphology (DBCM), University of Lausanne, 1005 Lausanne, Switzerland, [6]Central Institute for Experimental Animals, Kawasaki, Kanagawa 216-0001, Japan, [7]Keio Advanced Research Center, Keio University School of Medicine, Tokyo 160-8582, Japan, [8]Westfälische Wilhelms-Universität Münster, Zentrum für Molekularbiologie der Entzündung, Institute of Cell Biology, Stem Cell Biology and Regeneration Group, 48149 Münster, Germany and [9]RIKEN Brain Science Institute, RIKEN-Keio University Joint Research Laboratory, Wako, Saitama 351-0198, Japan

Isabel Reillo and Ayako Y. Murayama are joint second authors
Wieland B. Huttner and Víctor Borrell are joint corresponding senior authors

Address correspondence to Wieland B. Huttner. Email: huttner@mpi-cbg.de.

Subventricular zone (SVZ) progenitors are a hallmark of the developing neocortex. Recent studies described a novel type of SVZ progenitor that retains a basal process at mitosis, sustains expression of radial glial markers, and is capable of self-renewal. These progenitors, referred to here as basal radial glia (bRG), occur at high relative abundance in the SVZ of gyrencephalic primates (human) and nonprimates (ferret) but not lissencephalic rodents (mouse). Here, we analyzed the occurrence of bRG cells in the embryonic neocortex of the common marmoset *Callithrix jacchus*, a near-lissencephalic primate. bRG cells, expressing Pax6, Sox2 (but not Tbr2), glutamate aspartate transporter, and glial fibrillary acidic protein and retaining a basal process at mitosis, occur at similar relative abundance in the marmoset SVZ as in human and ferret. The proportion of progenitors in M-phase was lower in embryonic marmoset than developing ferret neocortex, raising the possibility of a longer cell cycle. Fitting the gyrification indices of 26 anthropoid species to an evolutionary model suggested that the marmoset evolved from a gyrencephalic ancestor. Our results suggest that a high relative abundance of bRG cells may be necessary, but is not sufficient, for gyrencephaly and that the marmoset's lissencephaly evolved secondarily by changing progenitor parameters other than progenitor type.

Keywords: brain evolution, cell cycle, gyrencephaly, marmoset, OSVZ

Introduction

A fundamental question in developmental neurobiology is how the expansion of the neocortex that occurred during the evolution of mammals is related to the types, numbers, and modes of division of cortical stem and progenitor cells (Rakic 1995, 2000, 2009; Kriegstein et al. 2006; Abdel-Mannan et al. 2008; Fish et al. 2008; Lui et al. 2011). These cells have been classified based on the location of their cell bodies, their site of mitosis, and the extent of cell polarity (Kriegstein and Alvarez-Buylla 2009; Fietz and Huttner 2011). The primary neural stem and progenitor cells in the neocortex, as elsewhere in the neural tube, are the neuroepithelial (NE) cells. NE cells exhibit apical–basal cell polarity, contact both apical (ventricular) and basal (pial) surfaces of the developing neocortex, their cell bodies constitute the ventricular zone (VZ), and their mitoses occur at the apical surface. With the onset of cortical neurogenesis, NE cells transform into the highly related radial glial (RG) cells. Because of their common site of mitosis, both NE and RG cells have been collectively referred to as apical progenitors (APs). APs undergo repeated symmetric and subsequently asymmetric divisions, indicative of a high potential for self-renewal (Götz and Huttner 2005; Pinto and Götz 2007; Kriegstein and Alvarez-Buylla 2009; Fietz and Huttner 2011).

A hallmark of the developing neocortex is the abundant occurrence of a second class of neural progenitors that divide in an abventricular (basal) location, which are referred to as basal progenitors (BPs) (Fietz and Huttner 2011) or intermediate progenitor cells (IPCs) (Kriegstein and Alvarez-Buylla 2009) and are typically found in the subventricular zone (SVZ) (Cheung et al. 2010). In lissencephalic rodents such as mouse and rat, BPs typically lack overt apical–basal cell polarity. The vast majority of rodent BPs divide only once in a self-consuming manner, generating 2 postmitotic neurons, which indicates their virtual lack of self-renewing potential (Kriegstein and Alvarez-Buylla 2009; Fietz and Huttner 2011).

Triggered by the seminal study of Smart et al. (2002) describing the cytoarchitectonic differences between the inner SVZ (ISVZ) and the outer SVZ (OSVZ) in primates, 3 laboratories independently reported on the main cell biological features of a novel neural progenitor type thought to be characteristic of the OSVZ (Fietz et al. 2010; Hansen et al. 2010; Reillo et al. 2011). These progenitors, referred to as OSVZ progenitors (Lukaszewicz et al. 2005; Fish et al. 2008; Fietz et al. 2010; Fietz and Huttner 2011; Shitamukai et al. 2011), outer RG cells (Hansen et al. 2010; Wang et al. 2011), or intermediate RG cells (Reillo et al. 2011), divide like rodent BPs in an abventricular (basal) location, typically the SVZ. However, in contrast to the vast majority of rodent BPs, these novel progenitor cells exhibit cell polarity, being monopolar cells that lack an apical process but retain a basal process at mitosis (Fietz and Huttner 2011). Other features that distinguish them from typical rodent BPs are the sustained expression of the transcription factors Pax6 and Sox2 and of RG cell markers and the lack of expression of the transcription factor Tbr2 (Fietz et al. 2010; Hansen et al. 2010; Reillo et al. 2011). As these progenitors are not confined to the OSVZ but also occur in the ISVZ of human (and ferret, see below) neocortex (Fietz et al. 2010; Reillo et al. 2011), we shall

refer to them henceforth as basal RG (bRG) cells rather than "OSVZ progenitors" or "outer RG."

bRG cells appear to be endowed with self-renewing potential, as they have been observed to undergo repeated asymmetric divisions (Hansen et al. 2010; Reillo et al. 2011). In fact, interference with extracellular matrix-induced integrin signaling was found to specifically reduce the pool size of bRG cells, suggesting that their potential for self-renewal may be linked to the retention of the basal process (Fietz et al. 2010).

While the OSVZ as a distinct layer in terms of cytoarchitecture, being separated from the ISVZ by an inner fiber layer, was originally suggested to be specific to the developing neocortex of primates (Smart et al. 2002), the cell biological characterization of bRG cells has revealed that their occurrence as such is not confined to primates. Thus, bRG progenitors have been observed in the developing neocortex of the ferret (Fietz et al. 2010; Reillo et al. 2011) and, very recently, the mouse (Shitamukai et al. 2011; Wang et al. 2011). Importantly, however, the abundance of bRG cells is strikingly different between the species analyzed so far. Whereas in the developing human and ferret neocortex bRG progenitors constitute about half of all mitotic SVZ progenitors (Fietz et al. 2010; Hansen et al. 2010; Reillo et al. 2011), they constitute only a minute fraction of mitotic SVZ progenitors in the developing mouse neocortex (Shitamukai et al. 2011; Wang et al. 2011). Given that human and ferret are gyrencephalic, whereas mouse is lissencephalic, these observations have raised the possibility that an abundant occurrence of bRG progenitors in the SVZ may be a characteristic feature of developing gyrencephalic (as opposed to lissencephalic) neocortex (Fietz et al. 2010; Reillo et al. 2011; Fietz and Huttner 2011). This possibility would be consistent with the notion that the potential of SVZ progenitors for self-renewal is linked to the retention of the basal process (Fietz et al. 2010).

A key question thus arising is: what is the abundance of bRG cells in the SVZ of a lissencephalic primate? To address this question, we have analyzed the neocortex of the common marmoset *Callithrix jacchus*, a near-lissencephalic primate, at various stages of embryonic development. We show that the abundance of bRG cells in the marmoset SVZ is similar to that in the developing gyrencephalic human and ferret neocortex, suggesting that a frequent occurrence of bRG cells, while perhaps necessary, is not sufficient, for gyrencephaly. Moreover, an evolutionary analysis suggests that the marmoset may have evolved from a gyrencephalic ancestor. Together, our data are consistent with the concept that changes in multiple parameters, including progenitor type and abundance as well as cell cycle kinetics and number, determine whether the neocortex develops to become lissencephalic or gyrencephalic.

Materials and Methods

Marmoset Embryos

Animal Maintenance and Timed Pregnancies

For embryonic stages E40 and E95, marmoset monkeys (*C. jacchus*) were raised in the institutional breeding facility of the Centre of Reproductive Medicine and Andrology (Bunk et al. 2011). Breeding, maintenance, and experimental procedures were performed in accordance with the German Federal Law on the Care and Use of Laboratory Animals. A license for the marmoset breeding colony was obtained from local authorities (Veterinär- und Lebensmittelüberwachungsamt der Stadt Münster). The license to sacrifice marmosets as tissue donors for scientific experiments was granted by the responsible review board: Landesamt für Natur, Umwelt und Verbraucherschutz Nordrhein-Westfalen (Permit number: 8.87-50.10.46.09.018). In accordance with the recommendations of the Weatherall report, "The use of non-human primates in research," every effort was made to alleviate animal discomfort and pain. The stages of marmoset embryos were determined on the basis of breeding time and embryo size.

For embryonic stages E78 and E92, fixed brains were provided by E.S. All animal experiments were approved by the institutional animal care and user committee and were performed in accordance with institutional guidelines for animal experiments. The ovarian cycles were synchronized using the prostaglandin F2α analog cloprostenol (0.75 mg/head Estrumate; Schering-Plough Animal Health, Union, NJ), which was administered in the luteal phase, 10 days after ovulation. Plasma samples (0.1 mL) were collected from the femoral vein at 9, 11, and 13 days after the injection of cloprostenol, and the day of ovulation was determined by measurement of plasma progesterone concentrations using an enzyme immunoassay (TOSO Progesterone Kit, TOSO, Tokyo, Japan) according to the manufacturer's protocol. Ovulation (day 0) was defined as the day prior to the rise of plasma progesterone levels above 10 ng/mL (Harlow et al. 1983). Embryos were collected 4–5 days after ovulation as previously described (Thomson et al. 1994). To obtain fetuses of uniform size, 2 embryos were nonsurgically transferred to surrogate mothers that were synchronized with regard to their ovulation cycles (Marshall et al. 1997).

For embryonic stages E85 and E100, fixed embryonic brains were obtained from the Wisconsin National Primate Center in Madison, WI (E85) and the German Primate Center in Götingen, Germany (E100). The stages of embryos were determined on the basis of breeding time and embryo size.

Sacrifice and Caesarean Section

For embryo stages E40 and E95, pregnant mothers were anesthetized with ketamin/xylazin and killed by exsanguination. Embryos were dissected, and the whole brain was removed from the skull. After dissection, the brains were immediately put in fixative.

For embryo stages E78 and E92, pregnant mothers were immobilized by intramuscular injection of 25 μg/head of atropine sulfate (0.5 mg/mL; Mitsubishi Tanabe Pharma Corporation, Osaka, Japan) and 70 mg/kg of ketamine hydrochloride (Veterinary Ketalar 50; Sankyo Lifetech Co., Ltd., Tokyo, Japan). Thereafter, animals were anesthetized by inhalation of 1–3% of isoflurane (Forane; Abbott Japan, Tokyo, Japan) via a ventilation mask. Anesthetization management was performed by spontaneous respiration during the operation, monitoring the heart rate and the arterial oxygen saturation. The uterus was exteriorized following midline laparotomy, and the proximal end of the uterus was incised for the Caesarean section. After the Caesarean section, the uterus, abdominal muscles, and skin were sutured. Embryonic brains were dissected in ice-cold phosphate-buffered saline (PBS), removing the meninges, and transferred to fixative.

Fixation

After dissection, marmoset E40 and E95 brains were immersed in 4% paraformaldehyde (PFA) (w/v) in PBS and left in fixative for 24 h at 4 °C with mild agitation. After fixation, the brains were kept at 4 °C in a mixture of 3 parts PBS containing 0.01% NaN_3 and 1 part 4% PFA in 120 mM sodium phosphate buffer pH 7.4.

For marmoset stages E78, E85, E92 and E100, the hemispheres were immersed in 4% PFA in phosphate buffer. The tissue was left at room temperature for an hour, transferred to 4 °C, and kept at that temperature with mild agitation. Brains were maintained in fixative for 24 h (E78, E92, and E100) or 3 months (E85) and then removed from fixative, rinsed in 120 mM phosphate buffer, transferred to 0.5% PFA in phosphate buffer containing 0.01% NaN_3, and kept at 4 °C until processed.

Immunohistochemistry

In addition to marmoset brains fixed as described above, E13.5 mouse brains and E39 and P1 ferret brains were obtained, PFA fixed and subjected to immunohistochemistry as described previously (Pulvers and Huttner 2009; Fietz et al. 2010; Arai et al. 2011). For cryosectioning,

fixed brains (marmoset, ferret) were cryoprotected, first in 15% sucrose in PBS and then in 30% sucrose in PBS at 4 °C. Brains were embedded in Tissue-Tek (Sakura Finetek) and stored at −20 °C. Sections were cut at 10 μm (marmoset E40), 12 μm (marmoset E78 and E92, ferret E39), and 20 μm (marmoset E95, ferret P1) and stored at −20 °C. For vibratome sectioning, fixed brains (marmoset, mouse, ferret) were embedded in 3% (marmoset E78, E92, E95, mouse E13.5, ferret E39) or 4% (marmoset E85) low-melting agarose in PBS, cut at 50 μm (marmoset E78, E92), 60 μm (marmoset E85), or 100 μm (marmoset E95, mouse E13.5, ferret E39), and stored in PBS with the addition of NaN_3 until further processing. Paraffin-embedded brains of marmoset E85 were cut at 5 μm and stored at room temperature until further processing. Cryotome sections of marmoset E100 tissue were cut at 50 μm.

Cryosections and paraffin sections were washed in PBS and subjected to antigen retrieval. Antigen retrieval was performed in a water bath in 0.01 M sodium citrate buffer (pH 6.0) supplemented with 10% (v/v) glycerol for 1 h at 70 °C. Free-floating vibratome sections were heated in 0.01 M sodium citrate buffer for 30 min at 85 °C. After heating, the sections were left standing in the antigen retrieval solution for 20 min at room temperature. Sections were then washed in PBS, permeabilized in 0.3% Triton X-100 (w/v) in PBS for 30 min at room temperature, quenched with 0.1 M glycine for 30 min at room temperature, and further subjected to immunocytochemistry as previously described (Kosodo et al. 2004). Primary antibodies were incubated overnight at 4 °C and secondary antibodies were incubated for 1 h at room temperature. The following primary antibodies were used: rabbit antibodies to Pax6 (Covance, PRB-278P, 1:200), Tbr2 (Abcam, ab23345, 1:200), Sox2 (Abcam, ab97959, 1:200), glutamate aspartate transporter (GLAST)-1 (Invitrogen, 42-8100, 1:200), proliferating cell nuclear antigen (PCNA) (Abcam, ab2426, 1:200), phosphohistone H3 (Millipore, 06-570, 1:200), Par3 (Millipore, 07-330, 1:200), Ki67 (Novocastra, NCL-Ki67p, 1:200); mouse monoclonal antibodies to phosphovimentin (Abcam, ab22651, 1:200), PCNA (Chemicon, MAB424, 1:100), glial fibrillary acidic protein (GFAP) clone G-A-5 (Sigma, G3893, 1:200), ZO-1 (Invitrogen, 33-9100, 1:200); goat polyclonal antibody to Sox2 (R&D Systems, AF2018, 1:100); and rat monoclonal antibody to phosphohistone H3 (Abcam, ab10543, 1:300). Donkey secondary antibodies coupled to Alexa 488, Alexa 555, or Alexa 647 were used (Molecular Probes, 1:500). All sections were counterstained with 4', 6-diamidino-2-phenylindole (DAPI) (Sigma, 1:500). Sections were mounted in Prolong Gold Antifade reagent (Invitrogen) and kept at 4 °C.

DiI Labeling

DiI labeling was performed as described (Fietz et al. 2010) with minor modifications. PFA-fixed vibratome sections (100 μm) of E95 marmoset neocortex in PBS were immobilized in a plastic dish using a metal grid (Warner Instruments). DiI (Vybrant Multicolor Cell-Labeling Kit, Molecular Probes) was injected under the meninges using a glass capillary and an Eppendorf Transjector (model 5246) attached to an InjectMan NI2 micromanipulator. Injection was performed under microscopic control (20×, Axiovert 200, Zeiss). Sections were incubated for 6 days in the dark in 4% PFA in 120 mM sodium phosphate buffer pH 7.4 at 37 °C. After incubation, sections were washed in PBS, stained with DAPI (1:500 in PBS, 1 h at room temperature), washed in PBS, and mounted as above.

Image Acquisition

Confocal images were acquired using a Zeiss LSM 710 or a Zeiss LSM 700 single-photon point-scanning confocal system using a 20×, 40×, or 63× objective or a confocal spectral microscope Leica SP2 AOBS. Images were taken as either 2.4 μm (20×), 1.2 μm (40×), or 0.9 μm (63×) single optical sections. Images taken as tile scans were stitched together using the ZEN software (Zeiss) or a stitching plug-in (Preibisch et al. 2009) in Fiji (http://pacific.mpi-cbg.de). Conventional fluorescence microscopy images were obtained using a Leica CTR5000 microscope. Quantifications were performed using Fiji software, ImageJ or Neurolucida. Images are oriented with the apical surface of the cortical wall facing downwards.

Determination of Layers in the Cortical Wall and Cell Counting

The VZ was identified as a densely packed cell layer lining the ventricle. The nuclei in this layer exhibited radial morphology, which was more prominent at earlier embryonic stages. The zone basally adjacent to the VZ, the SVZ/ISVZ, was identified by a less radial orientation of nuclei as compared with the VZ and by a distinct pattern of nuclear packing. The OSVZ was defined as a layer consisting of nuclei more radially aligned than the ones found in the ISVZ and was also distinguishable by a different nuclear density as compared with the ISVZ. The intermediate zone (IZ) was identified as a cell-sparse layer situated basally to the SVZ/OSVZ. Similarly, the subplate (SP) was distinguishable as a layer with distinct nuclear pattern basally to the IZ. The densely packed zone with distinct nuclear orientation located basally to the IZ or SP was identified as the cortical plate.

All cell counts were done using Fiji software and a specially developed Multiclass Cell Counter plug-in. The fluorescence signal was counted without using pseudocolor. Cell counting was confined to the dorsolateral telencephalon. Data were further processed using Prism software (GraphPad Software).

Comparative Phylogenetic Analysis

We collected the gyrification index (GI) values of 23 anthropoid species (Zilles et al. 1989). In addition, we calculated the GI values for 3 other anthropoid species—*Callicebus moloch*, *Alouatta palliata*, and *Mandrillus sphinx*—using data published at http://brainmuseum.org. The latter GI values were calculated as described previously (Zilles et al. 1988). We used 13–19 coronal Nissl-stained sections, equally spaced along the anterior–posterior axis of the brain. The outer and inner contours were traced in Fiji. The GI values of all species analyzed are listed in Supplementary Table 1.

To infer the ancestral GI values for these species, we required both phylogenetic topology and branch length information for the extant species because their membership in the nested hierarchy of a phylogeny implies that they are not statistically independent. Therefore, we assembled an anthropoid phylogeny using topology and branch lengths estimated previously (Perelman et al. 2011) based on ~8 Mb of genomic sequence (Supplementary Fig. 1; the tree file is available in Newick format in Supplementary File 1, with branch lengths equal to maximum likelihood estimates of the number of nucleotide substitutions per site). When only the genus was known for a particular GI value, we took the average species branch length for all members of that genus in the phylogeny. This phylogeny was then converted into an ultrametric chronogram in which the branch lengths are proportional to evolutionary time using the R package "APE" (Paradis et al. 2004).

The ancestral GI values were then estimated by fitting an evolutionary model to the GI values for the extant species. This model assumes that evolutionary change along each branch of the phylogeny follows a Brownian process in which the change in character value in any generation is independent of changes at prior generations (Felsenstein 1985). An additional assumption of the model is that there is a constant rate of evolution along each branch of the phylogeny. The model parameters were fitted by maximum likelihood (Schluter et al. 1997) using the ancestral character estimation (ace) function in APE.

Results

Abundant Occurrence of Pax6- and Sox2-Expressing Progenitor Cells in the E95 Marmoset SVZ

Given that Pax6 expression is one of the characteristic features of bRG cells (Fietz et al. 2010; Hansen et al. 2010; Reillo et al. 2011), we first examined the embryonic marmoset neocortex for the occurrence of Pax6-positive cells. At any of the 4 developmental stages investigated (E40, E78, E92, and E95), virtually all cells in the VZ, including cells undergoing mitosis at the ventricular surface, were Pax6 positive (Fig. 1*A*,*D*,*H*,*J*,*I*). These observations are consistent with the notion that marmoset neocortical APs express Pax6, as do neocortical APs in other mammals.

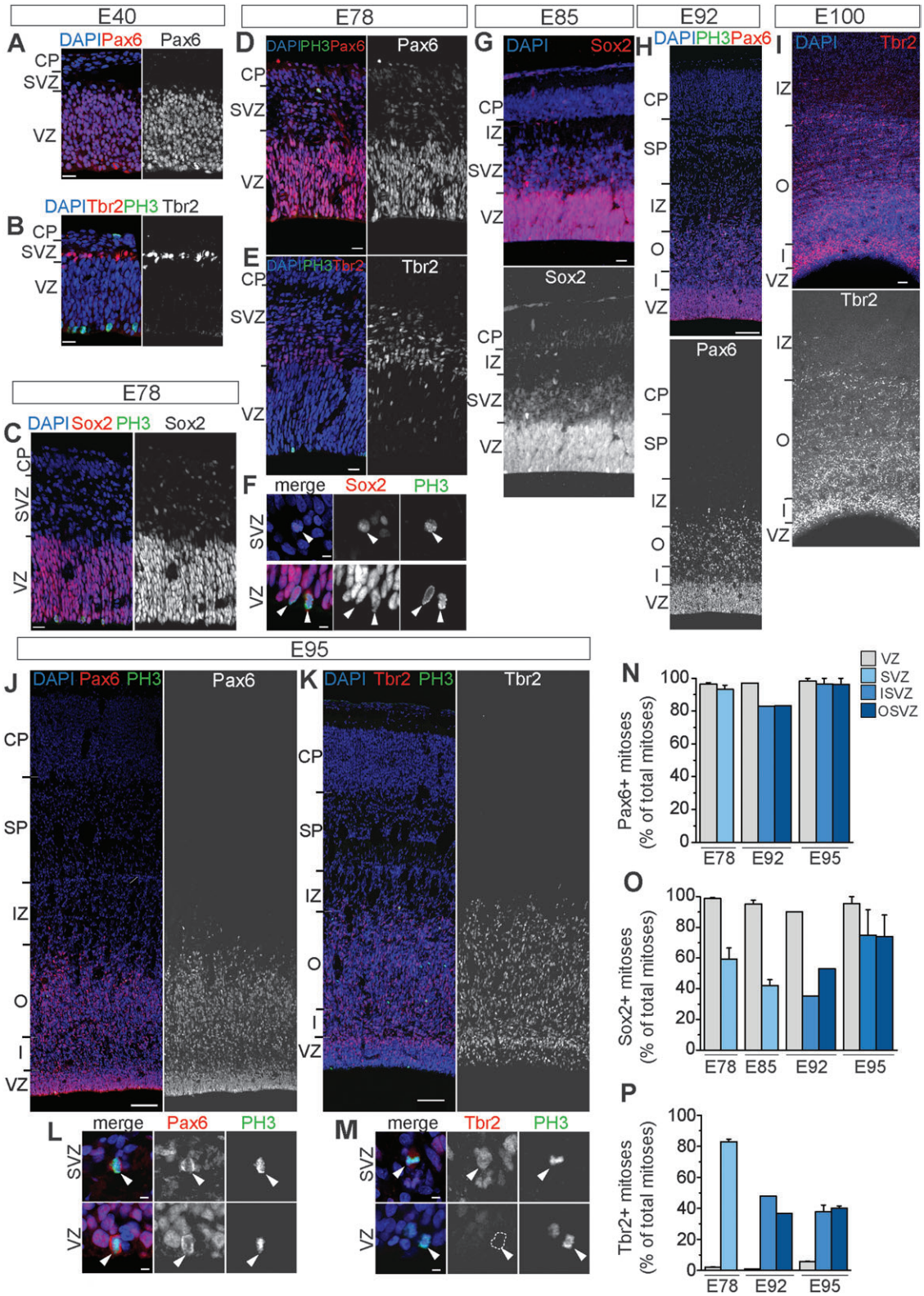

Figure 1. Distribution of Pax6-, Sox2-, and Tbr2-expressing progenitor cells in the VZ, SVZ, ISVZ, and OSVZ of marmoset neocortex at various embryonic stages. (*A*,*B*) E40, 10-μm cryosections. (*A*) Immunofluorescence for Pax6 (red/white). (*B*) Double immunofluorescence for Tbr2 (red/white) and phosphohistone H3 (PH3, green). (*C*–*F*) E78, 12-μm cryosections. Double immunofluorescence for Sox2 (red/white) and PH3 (green) (*C*), Pax6 (red/white) and PH3 (green) (*D*), and Tbr2 (red/white) and PH3 (green) (*E*). (*F*) Double immunofluorescence for Sox2 (red/white) and PH3 (green/white), showing selected mitotic progenitor cells (arrowheads) in the SVZ (top row) and VZ (bottom row) at higher magnification. (*G*) E85, 5-μm paraffin section. Immunofluorescence for Sox2 (red/white). (*H*) E92, 12-μm cryosection. Double immunofluorescence for Pax6 (red/white) and PH3 (green). (*I*) E100, 50-μm cryotome section. Immunofluorescence for Tbr2 (red/white). (*J*–*M*) E95, 20-μm cryosections. Double immunofluorescence for either Pax6 (red/white) (*J*,*L*) or Tbr2 (red/white) (*K*,*M*) and PH3 (green). Panels *L* and *M* show selected mitotic progenitor cells (arrowheads) in the SVZ (top row) and VZ (bottom row) at higher magnification; note the Tbr2-negative mitotic AP (dashed line). (*N*–*P*) Quantification of Pax6-positive (Pax6+) mitoses (*N*), Sox2-positive (Sox2+) mitoses (*O*), and Tbr2-positive

Regarding the SVZ, at E40, we observed a slender layer of nuclei basal to the VZ containing nuclei immunoreactive for the BP marker Tbr2 (Fig. 1*B*). This layer also appeared to contain a few Pax6-positive nuclei (Fig. 1*A*). However, the slenderness of this layer at this early developmental stage precluded determining whether the latter nuclei belonged to APs or bRG cells.

At E78, an SVZ was well discernible, with most nuclei being Tbr2 positive (Fig. 1*E*). Many of the nuclei in the E78 SVZ also showed Pax6 immunoreactivity, albeit at a lower level than the VZ nuclei (Fig. 1*D*). Immunostaining for the transcription factor Sox2, which is known to be expressed by neocortical APs (Ellis et al. 2004) and by human bRG cells (Hansen et al. 2010), revealed that many of the E78 SVZ nuclei were also Sox2 positive (Fig. 1*C*,*F*), albeit at a lower level than the VZ nuclei, as was the case for E85 SVZ nuclei (Fig. 1*G*).

At E92, E95, and E100, the thickness of the SVZ in the radial dimension had increased substantially and that of the VZ had decreased as compared with earlier developmental stages (Fig. 1*H*–*K*). Most, if not all, of the nuclei in the E92 and E95 SVZ showed Pax6 immunoreactivity, with the majority at a level similar to the VZ nuclei (Fig. 1*H*,*J*,*L*). Many of the E92 (data not shown), E95 (Fig. 1*K*,*M*), and E100 (Fig. 1*I*) SVZ nuclei were also Tbr2 positive.

To corroborate that the Pax6- and Sox2-positive cells in the embryonic marmoset SVZ were indeed progenitor cells, that is, undergoing mitoses, we quantified Pax6-positive and Sox2-positive mitoses and, for comparison, Tbr2-positive mitoses, as revealed by phosphohistone H3 immunostaining. Interestingly, at E92, the shape and distribution of nuclei across the SVZ was consistent with the existence of distinct layers reminiscent of an ISVZ and OSVZ (Fig. 1*H*; see also Fig. 4*D*), as described previously for other primates (Smart et al. 2002; Lukaszewicz et al. 2005; Fietz et al. 2010; Hansen et al. 2010; Reillo et al. 2011). The distinction between ISVZ and OSVZ became more obvious by E95 (Fig. 1*J*,*K*; see also Fig. 4*E*). Thus, in the apical region of the SVZ (amounting to approximately one-quarter to one-third of the entire SVZ), tentatively referred to as ISVZ, nuclei often exhibited a distinct pattern of packing and were less radially aligned than in the VZ. By contrast, in the basal region of the SVZ (amounting to approximately 3-quarters to two-thirds of the entire SVZ), tentatively referred to as OSVZ, nuclei exhibited a pattern of packing distinct from the ISVZ and appeared more radially aligned, resembling the VZ. For E92 and E95, we therefore separately quantified Pax6-, Sox2-, and Tbr2-positive mitoses for the ISVZ and OSVZ.

At E78 through E95, almost all mitoses at the ventricular surface of the VZ, that is, AP divisions, were Pax6 and Sox2 positive and Tbr2 negative (Fig. 1*N*–*P*), in line with data on neocortical APs in other mammals (Englund et al. 2005; Kowalczyk et al. 2009; Fietz et al. 2010; Hansen et al. 2010; Reillo et al. 2011; Arai et al. 2011). Remarkably, almost all mitoses in the E78 SVZ and E92–E95 ISVZ and OSVZ were Pax6 positive (Fig. 1*N*). Sox2-positive mitoses accounted for 40–60% of all mitoses in the E78–E85 SVZ and E92 ISVZ and OSVZ and increased to almost 80% in the E95 ISVZ and OSVZ (Fig. 1*O*). In contrast, the proportion of Tbr2-positive mitoses decreased from ≈80% in the E78 SVZ to ≈40% in the E92–E95 ISVZ and OSVZ (Fig. 1*P*). Together, these data raised the possibility that as much as about half of the progenitor cells in the embryonic marmoset SVZ are bRG cells (Pax6+/Sox2+/Tbr2–), which occurred at similar relative abundance in the ISVZ and OSVZ when these zones were discernible.

Marmoset SVZ Progenitor Cells Express Cytoplasmic Markers of RG

We sought to obtain further evidence in support of the RG nature of progenitor cells in the embryonic marmoset SVZ by immunostaining for GLAST and GFAP, 2 cytoplasmic markers of canonical RG cells (Kriegstein and Götz 2003) that have previously been shown to be also expressed in human and ferret bRG cells (Fietz et al. 2010; Hansen et al. 2010). At E78, we observed abundant GLAST immunoreactivity in the cell bodies of VZ progenitors, including mitotic cells at the ventricular surface (Fig. 2*A*,*B*), and in RG fibers extending toward the basal lamina (Fig. 2*A*). This indicated that RG cells in marmoset, as in other mammals, express GLAST. In addition, we could discern some cell bodies in the SVZ that were GLAST positive (Fig. 2*A*,*C*).

At E95, the occurrence of GLAST immunoreactivity in SVZ progenitor cell bodies was much more obvious and included mitotic cells (Fig. 2*D*,*F*), as was the case for the VZ (Fig. 2*D*,*E*). The evidence for the expression of RG markers in the SVZ was particularly strong in the case of GFAP, the level of immunoreactivity of which was higher in the SVZ than VZ (Fig. 2*D*–*F*). Together, these data indicate that a substantial proportion of progenitor cells in the marmoset E95 SVZ express cytoplasmic RG markers, consistent with them exhibiting properties of bRG cells.

A High Proportion of Progenitor Cells in the E95 Marmoset SVZ Retain a Basal Process at Mitosis

A hallmark of human and ferret bRG cells is the retention of a basal process throughout the cell cycle, including M-phase (Fietz et al. 2010; Hansen et al. 2010). If the abundantly occurring Pax6+/Sox2+/Tbr2–, cytoplasmic RG marker–expressing progenitors in the E95 marmoset SVZ were bRG cells, one would expect them to show basal process retention at M-phase. We investigated this by immunostaining vibratome sections for phosphovimentin, which has previously been used to detect basal processes of mitotic neural progenitors (Howard et al. 2006; Fietz et al. 2010; Hansen et al. 2010).

At E78 and E85, a phosphovimentin-positive basal process could be detected in only few of the mitotic progenitor cells in the SVZ, whereas such a process was frequently detected in the VZ (Fig. 3*A*–*F*,*I*). Interestingly, the frequency of mitotic progenitor cells retaining a basal process in the marmoset SVZ increased progressively from E78 to E95, with similar frequency in ISVZ and OSVZ when these zones were

(Tbr2+) mitoses (*P*) at E78, E85, E92, and E95 as indicated, each expressed as a percentage of total mitoses in the VZ (gray), SVZ (light blue), ISVZ (medium blue), and OSVZ (dark blue). Numbers of quantified cells (marker/total) were as follows: Pax6: E78 (2 brains) VZ 314/327, SVZ 45/48; E92 (1 brain) VZ 88/91, ISVZ 22/29, OSVZ 66/85; E95 (2 brains) VZ 65/66, ISVZ 53/55, OSVZ 101/105. Sox2: E78 (2 brains) VZ 200/201, SVZ 21/37; E85 (3 brains) VZ 356/375, SVZ 45/109; E92 (1 brain) VZ 55/61, ISVZ 6/17, OSVZ 26/49; E95 (2 brains) VZ 38/40, ISVZ 18/24, OSVZ 72/108. Tbr2: E78 (2 brains) VZ 8/393, SVZ 52/63; E92 (1 brain) VZ 1/106, ISVZ 23/48, OSVZ 54/147; E95 (2 brains) VZ 11/83, ISVZ 28/57, OSVZ 79/185. E85 Sox2: data are the mean of 3 brains, bars indicate standard error of the mean. E78, E95 Pax6, Sox2, and Tbr2: data are the mean of 2 brains, bars indicate the variation of the individual values from the mean. All sections were counterstained with DAPI (blue). Cortical plate (CP), SP, IZ, SVZ, OSVZ (O), ISVZ (I) and VZ are indicated. All panels except *G* and *I* are single optical sections: (*A*–*F*,*L*,*M*) 1.2 μm, (*H*,*J*,*K*) 2.4 μm. Scale bars: 5 μm (*F*,*L*,*M*), 20 μm (*A*–*E*,*H*), and 100 μm (*G*,*I*,*J*,*K*).

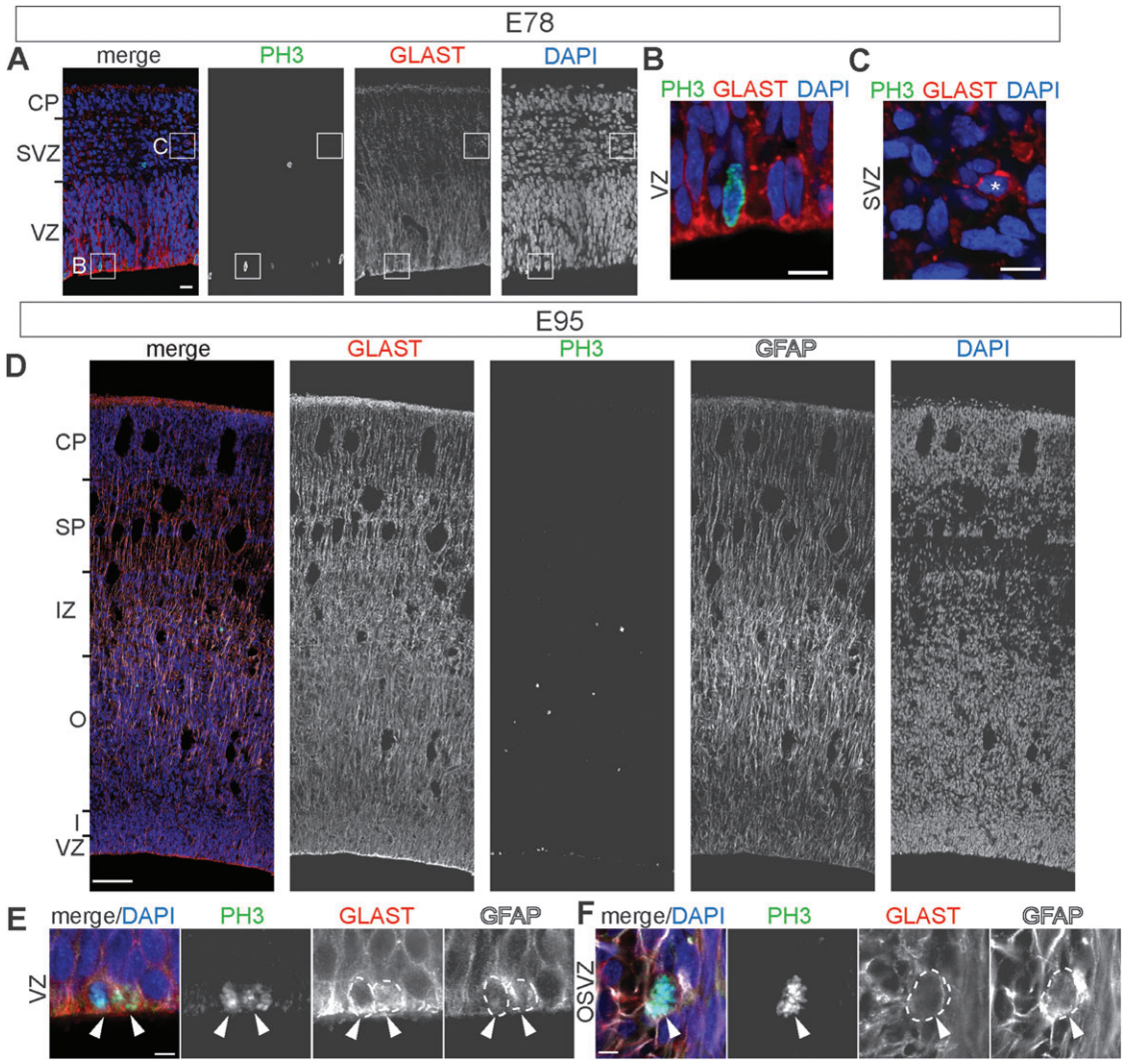

Figure 2. Expression of cytoplasmic markers of RG cells in SVZ progenitor cells of marmoset neocortex at various embryonic stages. (*A–C*) E78, 12-μm cryosection. Double immunofluorescence for phosphohistone H3 (PH3, green/white) and GLAST (red/white). Boxes in *A* indicate areas of the VZ and SVZ shown at higher magnification in *B* and *C*, respectively. Asterisk in *C* indicates a GLAST-expressing SVZ cell. (*D–F*) E95, 20-μm cryosections. Triple immunofluorescence for GLAST (red/white), PH3 (green/white), and GFAP (white). Arrowheads and dashed lines indicate cell bodies of mitotic cells at the ventricular surface (*E*) and in the OSVZ (*F*). All sections were counterstained with DAPI (blue/white). Cortical plate (CP), SP, IZ, SVZ, OSVZ (O), ISVZ (I), and VZ are indicated. All images are single optical sections: (*A–C*) 1.2 μm, (*D*) 2.4 μm, and (*E,F*) 0.9 μm. Scale bars: 10 μm (*B,C,E,F*), 20 μm (*A*), and 100 μm (*D*).

discernible (Fig. 3*L*). Thus, not only the majority of mitotic APs in the VZ but also about ≈35% of the mitotic progenitor cells in the ISVZ and OSVZ of E95 marmoset retained a phosphovimentin-positive basal process (Fig. 3*G–I,L*). Phosphovimentin immunostaining of cryotome sections indicated that this proportion increased to ≈50% for the E100 marmoset OSVZ (data not shown).

The basal process–bearing mitotic progenitor cells in the E95 marmoset VZ (Fig. 3*M*) and SVZ (Fig. 3*N*) were Pax6 positive but Tbr2 negative, as observed previously for ferret and human (Fietz et al. 2010; Hansen et al. 2010). Importantly, the abundance of basal process–retaining mitotic progenitor cells in the E95 marmoset SVZ was similar to that in the embryonic ferret and human SVZ (Fig. 3*O*) (Fietz et al. 2010; Hansen et al. 2010) and markedly different from that in the embryonic mouse SVZ, in which <5% of mitotic SVZ progenitor cells retain a basal process (Fig. 3*O*) (Shitamukai et al. 2011; Wang et al. 2011).

We used DiI labeling from the pial side of E95 marmoset neocortex to determine whether the basal processes emanating from cell bodies located in the SVZ actually reached the basal lamina. This revealed that such processes indeed extended all the way to the pial surface (Fig. 3*J,K*). Taken together, our data on the expression of transcription factors (Fig. 1) and RG markers (Fig. 2) as well as the presence of a basal process (Fig. 3*A–O*) indicate that bRG cells occur in the E95 marmoset SVZ at relatively high abundance.

Human and ferret bRG cells have previously been shown to lack apical cell polarity and an apical process extending to the ventricular surface (Fietz et al. 2010; Hansen et al. 2010; Reillo et al. 2011). The same was the case for E95 marmoset neocortex, as no apical process extending to the ventricular surface could be detected on DiI-labeled basal process–bearing SVZ cells (Fig. 3*J,K*). Moreover, immunostaining for Par3 and ZO-1, 2 apical polarity markers, revealed that E95 marmoset SVZ progenitors lacked apical polarity. Thus, Par3 and ZO-1 immunoreactivity was found to be clustered at the ventricular surface but was not detectable above background levels in the SVZ (Fig. 3*P*). We conclude that, as in the case of

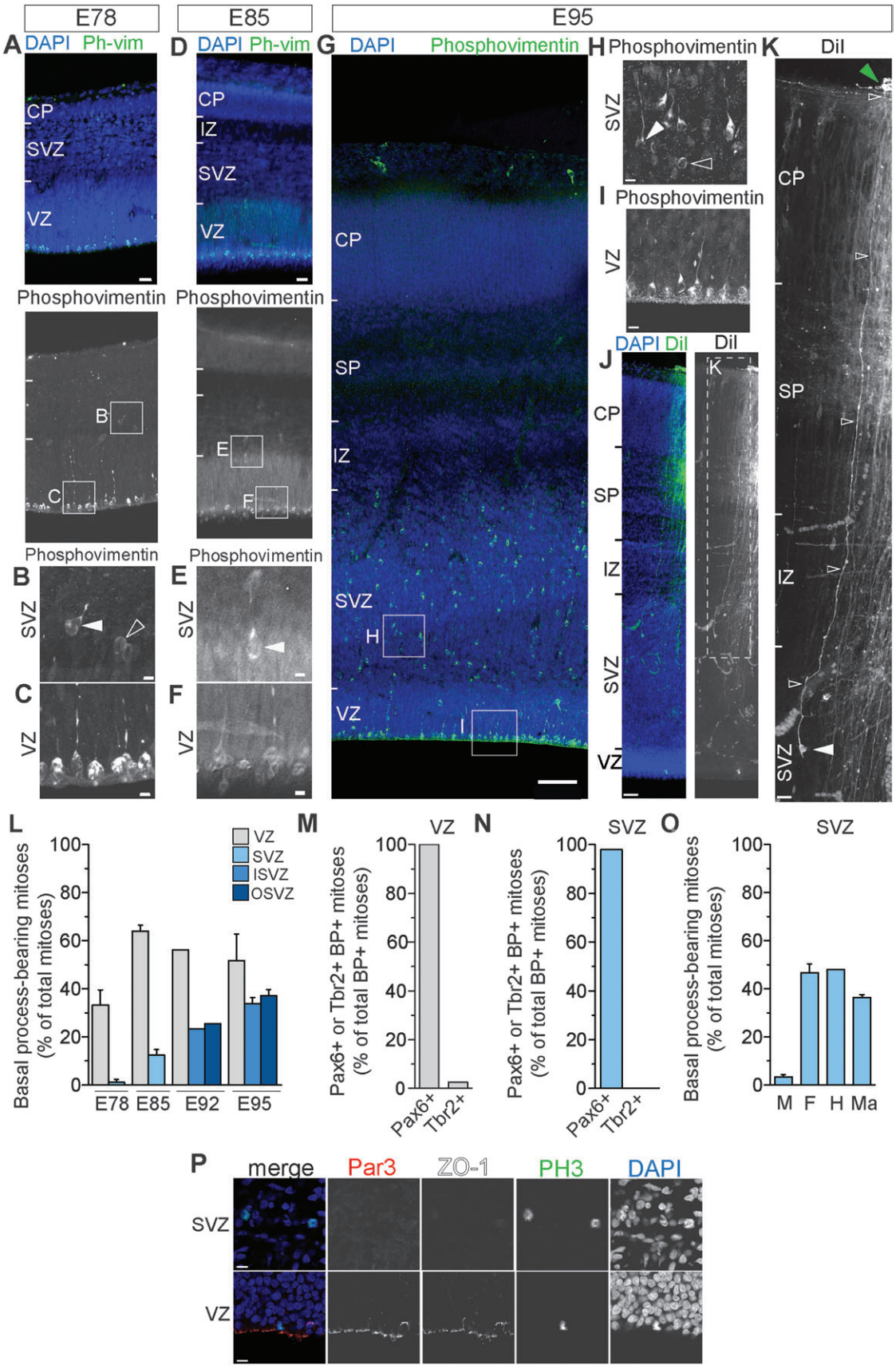

Figure 3. Occurrence of basal process–retaining progenitor cells in the SVZ of marmoset neocortex at various embryonic stages. (*A–C*) E78, 50-μm vibratome section. Immunofluorescence for phosphovimentin (Ph-vim, green/white). Boxes in *A* (lower panel) indicate areas of SVZ and VZ shown at higher magnification in *B* and *C*, respectively. Images are maximum intensity projection of 40 1.2 μm–thick single optical sections. Solid arrowhead, basal process–bearing mitotic progenitor cell in SVZ; open arrowhead,

human and ferret SVZ progenitor cells (Fietz et al. 2010; Hansen et al. 2010; Reillo et al. 2011), marmoset bRG cells are monopolar, exhibiting basal but not apical cell polarity (Fietz and Huttner 2011).

Cytoarchitecture of E92–E100 Marmoset Neocortex Reveals Existence of an ISVZ and OSVZ

The description, in a gyrencephalic primate, of the OSVZ as a distinct germinal zone in terms of cytoarchitecture (Smart et al. 2002) triggered the characterization of bRG cells as a novel type of neural progenitor as defined by marker expression and cell biological properties (Fietz et al. 2010; Hansen et al. 2010; Reillo et al. 2011). Given the abundant occurrence of bRG cells in the E95 marmoset SVZ, it was therefore of interest to examine whether the cytoarchitecture of the embryonic marmoset neocortex would be consistent with the existence of an OSVZ. Indeed, although the relative abundance of bRG cells in the apical versus basal regions of the E95 marmoset SVZ was essentially the same (Figs 1*N–P* and 3*L*), DAPI staining, as well as Tuj1 immunostaining, revealed a cytoarchitecture in the E95–E100 marmoset SVZ (corroborated as a germinal layer by PH3, phosphovimentin, PCNA, and/or Ki67 immunostaining [data not shown]) that was reminiscent of an ISVZ and an OSVZ, each characterized by a distinct pattern of nuclear packing and alignment (see above) (Fig. 4*E–I*). At E92, ISVZ and OSVZ started to become discernible (Fig. 4*D*). At the earlier embryonic stages at which the marmoset SVZ was less developed, such distinct zones were not obvious (Fig. 4*A–C*). Our data are consistent with the presence of ISVZ- and OSVZ-like zones in the E92–E100 marmoset neocortex (even if not all criteria of the original definition [Smart et al. 2002] may be fulfilled). However, although bRG cells were originally thought to be characteristic of the OSVZ (Smart et al. 2002; Fietz et al. 2010; Hansen et al. 2010; Reillo et al. 2011; Fietz and Huttner 2011), in light of the data on the quantification of bRG cells in the E95 ISVZ versus OSVZ (Figs 1*N–P* and 3*L*), we further conclude that the existence of an OSVZ does not allow to make predictions as to the abundance, in the ISVZ versus OSVZ, of bRG cells as defined by marker expression and cell biological properties.

Reduced Abundance of Progenitor Cells in M-Phase in the Embryonic Marmoset Neocortex

In the above shown phosphohistone H3 immunostainings used to identify progenitor cells in mitosis, we had noticed a relative scarcity of mitotic progenitors in single optical sections of the marmoset VZ and SVZ (Figs 1 and 2). We therefore quantified the proportion of cycling cells and of cells in M-phase in the VZ and SVZ of E78, E92, and E95 marmoset and, for comparison, of E39 and P1 ferret, which contains the same principal types of progenitor cells at similar abundance and develops a brain of similar size.

For the embryonic marmoset VZ, the proportion of cycling cells, as revealed by PCNA immunostaining (Fig. 5*A,B*), was found to be at least as high as for the VZ in the developing ferret neocortex (Fig. 5*D*). In the marmoset SVZ, the proportion of cycling cells was even higher than in the ferret SVZ (Fig. 5*D*). By contrast, the proportion of cells in M-phase, as revealed by phosphohistone H3 immunostaining (Fig. 5*A,B*), was lower in the E95 marmoset VZ and SVZ than in the VZ and SVZ, respectively, of developing ferret neocortex (Fig. 5*C*). Accordingly, the marmoset VZ and SVZ exhibited a markedly lower level of cells in M-phase when expressed as a proportion of cycling (PCNA-positive) cells than the ferret VZ and SVZ (Fig. 5*E*). The same was the case when another marker of cycling cells, Ki67, was used as denominator (Fig. 5*F*). On the assumption that the length of M-phase is similar for marmoset and ferret neocortical progenitor cells, these data would suggest that the cell cycle of marmoset neocortical progenitor cells is longer than that of ferret.

Ancestral GI Estimates Suggest that the Marmoset May Be Secondarily Lissencephalic

The data obtained on the abundance of bRG cells in the developing marmoset neocortex (Figs 1–3) prompted us to explore the possibility that the lissencephaly of the marmoset may be a secondary trait, that is, may have evolved from gyrencephaly along the lineage leading to *C. jacchus*. To this end, we first collected or determined the GIs of 26 extant anthropoid species (Supplementary Table 1). We then inferred the putative GI values of the ancestors of these species by fitting an evolutionary model to the GI values of the latter (Fig. 6). This yielded an estimated GI value of 1.75 ± 0.21 for the

mitotic progenitor cell in SVZ lacking a basal process. Note basal processes emanating from mitotic APs in *C*. (*D–F*) E85, 60-μm vibratome section. Immunofluorescence for phosphovimentin (Ph-vim, green/white). Boxes in *D* (lower panel) indicate areas of SVZ and VZ shown at higher magnification in *E* and *F*, respectively. Images were obtained by conventional fluorescence microscopy. Solid arrowhead, basal process–bearing mitotic progenitor cell in SVZ. Note basal processes emanating from mitotic APs in *F*. (*G–I*) E95, 100-μm vibratome section. Immunofluorescence for phosphovimentin (green/white). Boxes in *G* indicate areas of SVZ and VZ shown at higher magnification in *H* and *I*, respectively. Images are maximum intensity projection of 21 2.4 μm–thick single optical sections. Solid arrowhead, basal process–bearing mitotic progenitor cell in SVZ; open arrowhead, mitotic progenitor cell in SVZ lacking a basal process. Note basal processes emanating from mitotic APs in *I*. (*J,K*) E95, 100-μm vibratome section. DiI labeling (green/white) from pial side (green arrowhead). Dashed box in *J* (right panel) indicates the area of the cortical wall shown at higher magnification in *K*. Note the cell body (solid arrowhead) in the SVZ extending a basal process (open arrowheads) to the pial surface. Images are maximum intensity projection of 26 2.4 μm–thick single optical sections. (*A,D,G,J*) All sections were counterstained with DAPI (blue). Cortical plate (CP), SP, IZ, SVZ, and VZ are indicated. (*L*) Quantification, after phosphovimentin immunostaining, of basal process–bearing mitotic cells in the VZ (gray), SVZ (light blue), ISVZ (medium blue), and OSVZ (dark blue) at E78, E85, E92, and E95. Basal process–bearing mitoses are expressed as a percentage of total mitoses in the respective layer. Numbers of quantified cells (basal process bearing/total) were as follows: E78 (2 brains) VZ 164/446, SVZ 1/51; E85 (3 brains) VZ 380/598, SVZ 7/49; E92 (1 brain) VZ 83/148, ISVZ 7/30, OSVZ 36/141; E95 (2 brains) VZ 175/303, ISVZ 76/229, OSVZ 242/633. E85: data are the mean of 3 brains, bars indicate standard error of the mean (SEM); E78, E95: data are the mean of 2 brains, bars indicate the variation of the individual values from the mean. (*M,N*) Quantification of Pax6 (left bars) and Tbr2 (right bars) expression in phosphovimentin-immunostained basal process–bearing cells in the E95 VZ (gray, *M*) and SVZ (light blue, *N*). Data are from one brain. Numbers of quantified cells (Pax6+ or Tbr2+ basal process–bearing (BP+) mitoses/total BP+ mitoses) were as follows: Pax6 VZ 91/91, SVZ 48/49; Tbr2 VZ 1/38, 0/36. (*O*) Comparison of the relative abundance of basal process–bearing mitotic cells in the SVZ of E13.5 mouse, E39 ferret, 13wpc human, and E95 marmoset. Basal process–bearing mitoses are expressed as a percentage of total mitoses. Numbers of quantified cells (basal process bearing/total) were as follows: mouse E13.5 (4 brains) 17/431, ferret E39 (1 brain) 49/104, and marmoset E95 (2 brains) 318/862. Mouse E13.5 (*M*): data are the mean of 4 brains, bars indicate SEM; ferret E39 (*F*): data are the mean of 3 sections from one brain, bars indicate SEM; marmoset E95 (Ma): data are the mean of 2 brains, bars indicate the variation of the individual values from the mean. Data for human 13wpc (*H*) were taken from Figure 3*d* of Fietz et al. (2010). (*P*) E95, 20-μm cryosection. Triple immunofluorescence for Par3 (red/white), ZO-1 (white), and phosphohistone H3 (PH3, green/white), combined with DAPI staining (blue/white). Upper row, SVZ; lower row, VZ. Note the concentration of markers of apical polarity at the apical surface. Images are 1.2 μm–thick single optical sections. Scale bars: 5 μm (*B,C,E,F,H,I*), 10 μm (*P*), 20 μm (*A,D,K*), 50 μm (*J*), and 100 μm (*G*).

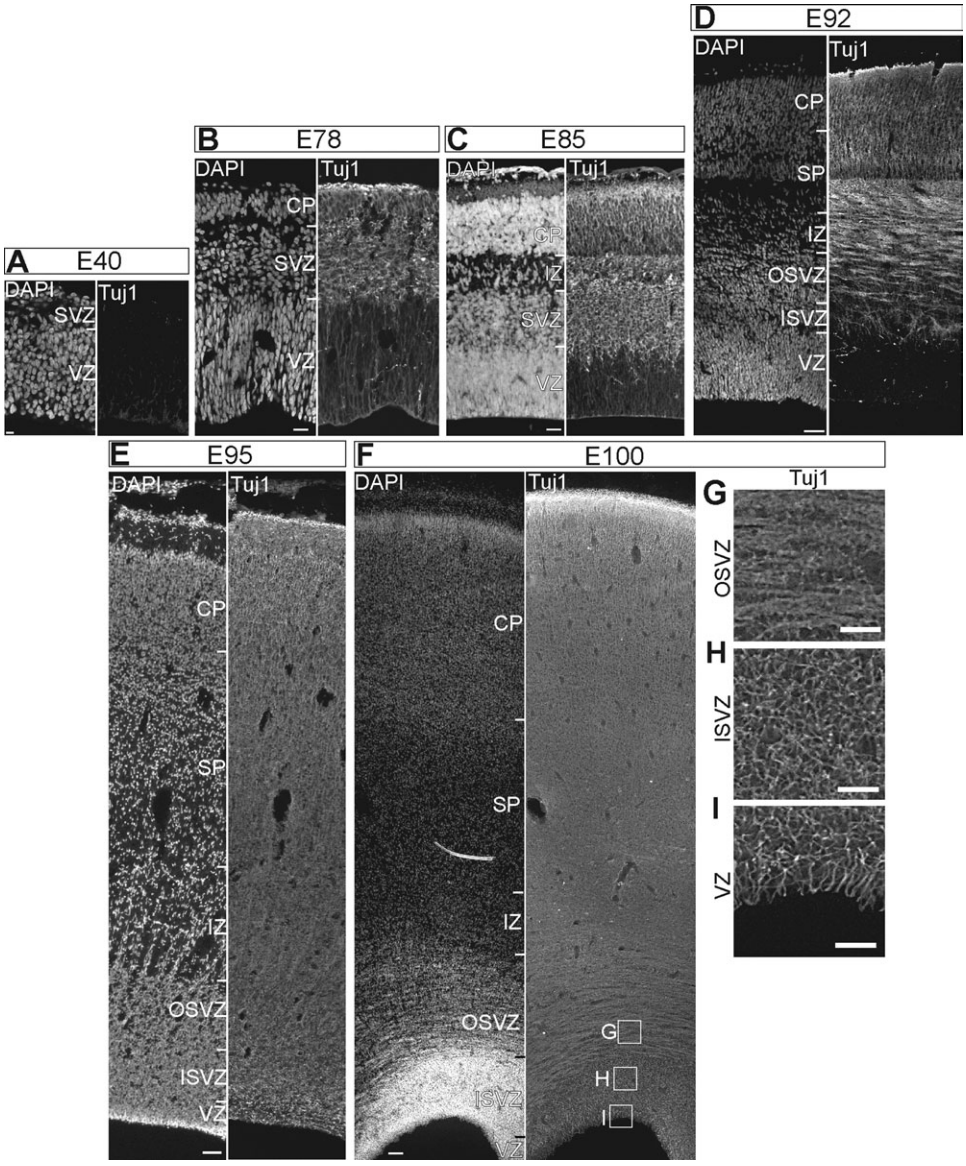

Figure 4. Cytoarchitecture of marmoset neocortex at various embryonic stages. Immunofluorescence for βIII-tubulin (Tuj1, right panels) combined with DAPI staining (left panels) at E40 (*A*, 10-μm cryosection), E78 (*B*, 12-μm cryosection), E85 (*C*, 5-μm paraffin section), E92 (*D*, 12-μm cryosection), E95 (*E*, 20-μm cryosection), and E100 (*F–I*, 50-μm cryotome section). Boxes in *F* (right panel) indicate areas of OSVZ, ISVZ, and VZ shown at higher magnification in *G*, *H*, and *I*, respectively. Cortical plate (CP), SP, IZ, SVZ, OSVZ, ISVZ, and VZ are indicated. Images are 1.2 μm–thick single optical sections (*A*,*B*,*D*) or are conventional fluorescence microscopy images (*C*,*E–I*). Scale bars: 10 μm (*A*), 20 μm (*B*,*C*), 50 μm (*D*,*G–I*), and 100 μm (*E*,*F*).

ancestor of the 26 anthropoid species compared with the GI value of 1.17 observed for *C. jacchus* (see Supplementary Table 2). These data are consistent with the possibility that during primate evolution, gyrencephaly may have been secondarily lost in certain lineages including that leading to *C. jacchus*.

Discussion

Our study shows that bRG cells occur in the SVZ of marmoset, a near-lissencephalic primate, at much greater relative abundance than in the SVZ of mouse (Shitamukai et al. 2011; Wang et al. 2011), a lissencephalic rodent, and at similar relative abundance as in the SVZ of human (Fietz et al. 2010; Hansen et al. 2010), a gyrencephalic primate, and ferret (Fietz et al. 2010; Reillo et al. 2011), a gyrencephalic nonprimate. Previously, the possibility has been discussed that the occurrence of bRG cells in the SVZ at high relative abundance may be an underlying cause of gyrencephaly (Fietz et al. 2010; Reillo et al. 2011; Fietz and Huttner 2011). In this regard, the present data leave us with 2 principal lines of interpretation. First, an abundance of bRG cells may not be linked to the appearance of gyrencephaly. Second, an abundance of bRG cells may be related to the appearance of gyrencephaly, but this relationship is more complex than previously assumed. Specifically, our findings are consistent with the concept that an abundance of bRG cells may be necessary, but is not sufficient, for gyrencephaly, as will be discussed below.

It has been known that the occurrence of bRG cells at high relative abundance does not correlate with the extent of gyrencephaly and of neocortical expansion in general. Thus, bRG cells occur at similar relative abundance in the embryonic

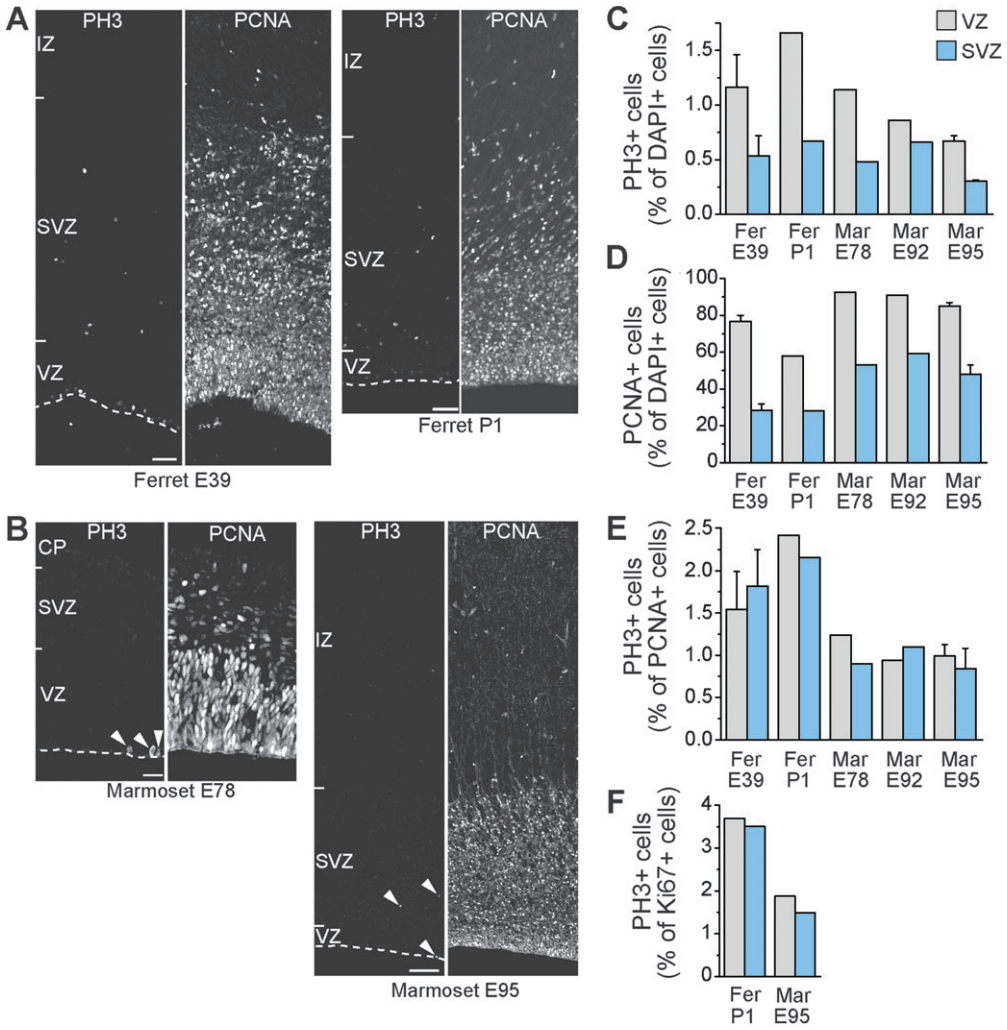

Figure 5. Comparison of cycling cells and cells in M-phase in embryonic marmoset and embryonic/postnatal ferret neocortex. (*A*,*B*) Double immunofluorescence for phosphohistone H3 (PH3) and PCNA of (*A*) E39 (left, 12-μm cryosection) and P1 (right, 20-μm cryosection) ferret neocortex and (*B*) E78 (left, 12-μm cryosection) and E95 (right, 20-μm cryosection) marmoset neocortex. All sections were counterstained with DAPI for quantification (data not shown). Cortical plate (CP), IZ, SVZ, and VZ, as well as ventricular surface (dashed lines), are indicated on PH3 images. Except for marmoset E78, the top margin of the images corresponds to the boundary between IZ and SP/CP. Arrowheads in *B* indicate PH3-positive cells. All images are 1.2 μm– (*B*, left) or 2.4 μm–thick (*A*,*B*, right) single optical sections. Scale bars: 20 μm (*B*, left), 50 μm (*A*), and 100 μm (*B*, right). (*C*–*F*) Quantification of cycling and mitotic cells in the VZ (gray) and SVZ (blue) of E39 (2 brains) and P1 (1 brain) ferret (Fer) and E78 (1 brain), E92 (1 brain), and E95 (*C*–*E*, 2 brains; *F*, 1 brain) marmoset (Mar) neocortex. (*C*) Quantification of PH3-positive (PH3+) cells, expressed as percentage of DAPI-stained (DAPI+) cells. Numbers of quantified cells (PH3+/DAPI+) were as follows: Ferret E39 VZ 17/1392, SVZ 14/2850; ferret P1 VZ 19/1140, SVZ 16/2374; marmoset E78 VZ 58/5050, SVZ 14/2904; marmoset E92 VZ 31/3604, SVZ 38/5694; marmoset E95 VZ 21/3239, SVZ 35/11226. (*D*) Quantification of PCNA-positive (PCNA+) cells, expressed as percentage of DAPI-stained (DAPI+) cells. Numbers of quantified cells (PCNA+/DAPI+) were as follows: Ferret E39 VZ 1060/1392, SVZ 788/2850; ferret P1 VZ 1351/2335, SVZ 1877/6646; marmoset E78 VZ 4602/4915, SVZ 1190/2224; marmoset E92 VZ 3278/3604 SVZ 3377/5694; marmoset E95 VZ 2138/3239, SVZ 3903/11226. (*E*) Quantification of PH3-positive (PH3+) cells, expressed as percentage of PCNA-positive (PCNA+) cells. Numbers of quantified cells (PH3+/PCNA+) were as follows: Ferret E39 VZ 17/1060, SVZ 14/788; ferret P1 VZ 19/785, SVZ 16/739; marmoset E78 VZ 58/4602, SVZ 10/1190; marmoset E92 VZ 31/3278 SVZ 38/3377; marmoset E95 VZ 21/2138, SVZ 35/3903. (*F*) Quantification of PH3-positive (PH3+) cells, expressed as percentage of Ki67-positive (Ki67+) cells. Numbers of quantified cells (PH3+/Ki67+) were as follows: Ferret P1 VZ 18/487, SVZ 23/655; marmoset E95 VZ 6/318, SVZ 13/868. E39 ferret and E95 marmoset (*C*–*E*): data are the mean of 2 brains, bars indicate the variation of the individual values from the mean.

ferret and human SVZ (≈50% in either species) (Fietz et al. 2010; Hansen et al. 2010; Reillo et al. 2011), yet the extent of gyrencephaly in these 2 mammals is vastly different. It follows that other parameters, such as the number of cell cycles that each bRG cell undergoes and/or the population size and cell cycle number of progenitor cells downstream of bRG cells (Hansen et al. 2010), critically determine the extent of gyrencephaly and of neocortical expansion.

Nonetheless, our study offers a possible explanation to reconcile the near-lissencephalic shape of the marmoset neocortex with the occurrence of bRG cells in the SVZ at similar abundance as in the gyrencephalic ferret and human neocortex. Specifically, the marmoset neocortex may be secondarily lissencephalic, perhaps reflecting the marmoset's relatively small body size. In other words, the marmoset may have evolved from a gyrencephalic ancestor by phyletic dwarfing (Ford 1980) and, due to the reduction in body size, may have been able to retain the same cortical surface-to-body volume ratio as its ancestor by developing a lissencephalic neocortex. Indeed, our analysis of the relationship between various anthropoid species with regard to their GI suggests that a common ancestor of these species would have exhibited a medium-level gyrencephalic neocortex, with some anthropoid species including marmoset subsequently becoming less gyrencephalic and others including human

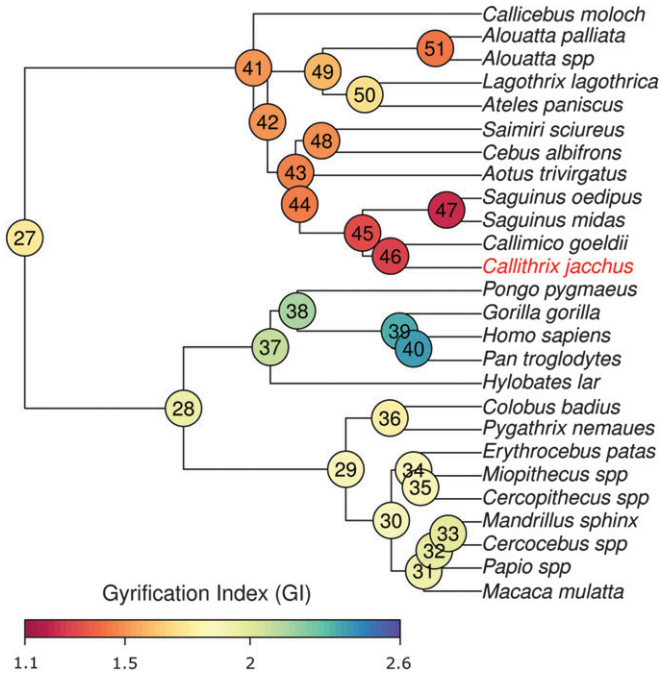

Figure 6. GI estimates for the ancestors of 26 anthropoid species. Ancestral GI values are indicated by colored circles at the root and internal nodes of the phylogeny (see color scale at bottom). For details, see Materials and Methods. Numbers in colored circles refer to node numbers (for the GI values associated with these nodes, see Supplementary Table 2), and branches are drawn proportional to time. The marmoset species analyzed in this study (*Callithrix jacchus*) is highlighted in red.

becoming more gyrencephalic (Fig. 6). Thus, while the marmoset's lissencephaly has been viewed as a primitive trait (Stellar 1960), our evolutionary model suggests that it may well be a derived trait. As a corollary of our concept, an abundance of bRG cells may well be characteristic of primates and other gyrencephalic species if one assumes that this abundance in the near-lissencephalic marmoset neocortex is counteracted by changes in other progenitor cell parameters.

Candidates for such parameters include the population size of neurogenic progenitor cells and the number of neurogenic divisions that each of these progenitor cells undergoes. In this context, we found that the proportion of cycling cells that were in M-phase was lower in embryonic marmoset than developing ferret neocortex. On the assumption that M-phase comprises a similar proportion of the cell cycle in marmoset and ferret neocortical progenitor cells, these data raise the possibility that the cell cycle of marmoset neocortical progenitor cells may be longer than that of ferret. Given that alterations in cell cycle length have been implicated in cortical development and expansion (Götz and Huttner 2005; Dehay and Kennedy 2007), it will be important to directly determine the cell cycle length of marmoset neocortical progenitors and compare it with other, lissencephalic and gyrencephalic, primate and nonprimate species.

Another candidate parameter contributing to lissencephaly versus gyrencephaly may be the time course of the change in the relative proportion of SVZ progenitor cells to VZ progenitor cells during neocortical development. Analyzing previous (Fietz et al. 2010) and present data, we noticed that the preponderance of the SVZ over the VZ in terms of radial thickness follows a different time course in embryonic marmoset compared with embryonic human or ferret (Fig. 7).

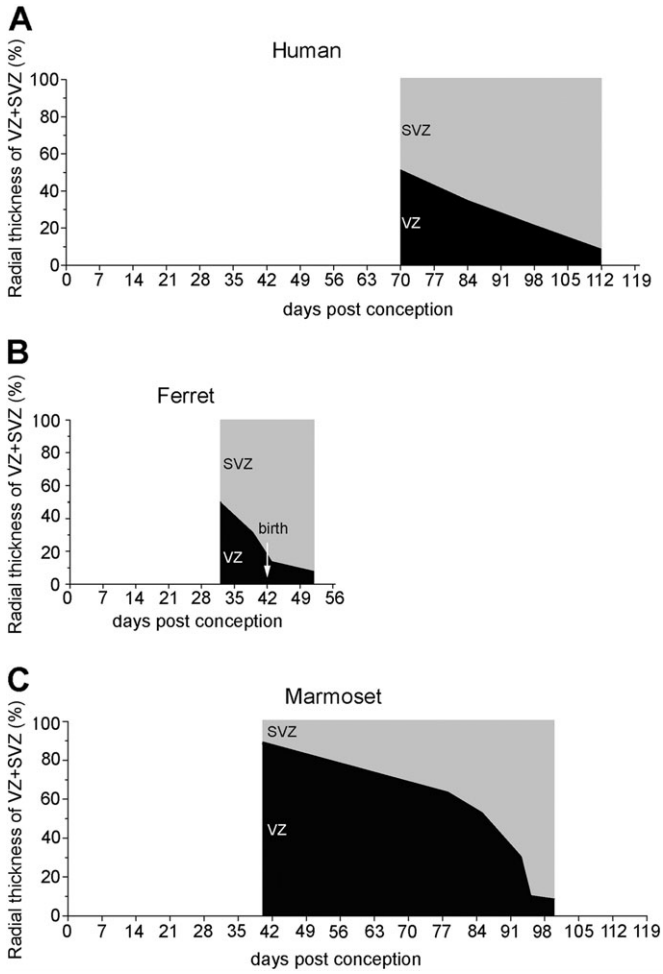

Figure 7. Radial thickness ratio of SVZ/VZ during embryonic development of human, ferret, and marmoset neocortex. Radial thickness of the VZ and SVZ was measured using the images shown in Figure 1*d–k* (human, *A*) and Figure 1*n–s* (ferret, *B*) of Fietz et al. (2010) and Figure 4*A–F* (marmoset, *C*). At each developmental stage, radial thickness values of the VZ (black areas) and SVZ (gray areas) are expressed as percentage of the sum of VZ + SVZ.

At E92, and even more so at E95 and E100, the cytoarchitecture of the marmoset SVZ, as apparent from DAPI and Tuj1 stainings, allowed us to distinguish between an ISVZ and an OSVZ. Yet, the relative abundance of bRG cells, as apparent from basal process–bearing/Sox2-positive/Tbr2-negative mitoses, was essentially the same for ISVZ and OSVZ. This not only underscores that referring to these progenitor cells as bRG cells rather than OSVZ progenitors or outer RG appears to be appropriate. It also reveals that cytoarchitecture does not necessarily allow one to make reliable predictions as to the abundance of a given progenitor type.

On a more general note, our study constitutes an effort to trace the origins of gross morphological features of the brain to fundamental cellular properties. Our results are consistent with the notion that gyrencephaly may be an evolutionarily labile trait, reflecting, perhaps, the relative ease with which neural progenitor cell parameters can be modified. This notion would be in line with the view that evolution often is a process of "tinkering" with available modules rather than inventing de novo (Jacob 1977). Given that transgenic techniques for the common marmoset have recently been developed (Sasaki et al.

2009), the significance of bRG cells for the development of the marmoset neocortex can be addressed by genetic manipulation in the future.

Supplementary Material

Supplementary material can be found at: http://www.cercor.oxfordjournals.org/

Funding

I.R. was supported by an Formación de Profesorado Universitario predoctoral fellowship from the Spanish Ministry of Science and Innovation (MICINN). This work was supported by the Strategic Research Program for Brain Sciences from the Ministry of Education, Culture, Sports, Science and Technology (MEXT), Japan to E.S. and H.O. and by "Funding Program for World-leading Innovative R&D on Science and Technology" to E.S. and H.O. W.B.H. was supported by grants from the Deutsche Forschungsgemeinschaft (DFG) (SFB 655, A2; TRR 83, Tp6) and the European Research Council (250197), by the DFG-funded Center for Regenerative Therapies Dresden, and by the Fonds der Chemischen Industrie. V.B. was supported by grants from the International Human Frontier Science Program Organization (CDA0027/2007-C), MICINN (SAF2009-07367), and CONSOLIDER (CSD2007-00023).

Notes

We thank J. Schindelin for developing the Fiji plug-in, S. Fietz for providing ferret brains and for helpful comments on the manuscript, J. Helppi and other members of the animal facility, and the light microscopy facility, of the Max Planck Institute of Molecular Cell Biology and Genetics for excellent support, and C. Vegar from the Instituto de Neurociencias for outstanding technical support. I.K. was a member of the International Max Planck Research School for Molecular Cell Biology and Bioengineering. *Conflict of Interest* : None declared.

References

Abdel-Mannan O, Cheung AF, Molnar Z. 2008. Evolution of cortical neurogenesis. Brain Res Bull. 75:398–404.

Arai Y, Pulvers JN, Haffner C, Schilling B, Nusslein I, Calegari F, Huttner WB. 2011. Neural stem and progenitor cells shorten S-phase on commitment to neuron production. Nat Commun. 2:154.

Bunk EC, Stelzer S, Hermann S, Schafers M, Schlatt S, Schwamborn JC. 2011. Cellular organization of adult neurogenesis in the common marmoset. Aging Cell. 10:28–38.

Cheung AF, Kondo S, Abdel-Mannan O, Chodroff RA, Sirey TM, Bluy LE, Webber N, DeProto J, Karlen SJ, Krubitzer L, et al. 2010. The subventricular zone is the developmental milestone of a 6-layered neocortex: comparisons in metatherian and eutherian mammals. Cereb Cortex. 20:1071–1081.

Dehay C, Kennedy H. 2007. Cell-cycle control and cortical development. Nat Rev Neurosci. 8:438–450.

Ellis P, Fagan BM, Magness ST, Hutton S, Taranova O, Hayashi S, McMahon A, Rao M, Pevny L. 2004. SOX2, a persistent marker for multipotential neural stem cells derived from embryonic stem cells, the embryo or the adult. Dev Neurosci. 26:148–165.

Englund C, Fink A, Lau C, Pham D, Daza RA, Bulfone A, Kowalczyk T, Hevner RF. 2005. Pax6, Tbr2, and Tbr1 are expressed sequentially by radial glia, intermediate progenitor cells, and postmitotic neurons in developing neocortex. J Neurosci. 25:247–251.

Felsenstein J. 1985. Phylogenies and the comparative method. Am Nat. 125:1–15.

Fietz SA, Huttner WB. 2011. Cortical progenitor expansion, self-renewal and neurogenesis-a polarized perspective. Curr Opin Neurobiol. 21:23–35.

Fietz SA, Kelava I, Vogt J, Wilsch-Bräuninger M, Stenzel D, Fish JL, Corbeil D, Riehn A, Distler W, Nitsch R, et al. 2010. OSVZ progenitors of human and ferret neocortex are epithelial-like and expand by integrin signaling. Nat Neurosci. 13:690–699.

Fish JL, Kennedy H, Dehay C, Huttner WB. 2008. Making bigger brains—the evolution of neural-progenitor-cell division. J Cell Sci. 121:2783–2793.

Ford SM. 1980. Callitrichids as phyletic dwarfs, and the place of the Callitrichidae in Platyrrhini. Primates. 21:31–34.

Götz M, Huttner WB. 2005. The cell biology of neurogenesis. Nat Rev Mol Cell Biol. 6:777–788.

Hansen DV, Lui JH, Parker PR, Kriegstein AR. 2010. Neurogenic radial glia in the outer subventricular zone of human neocortex. Nature. 464:554–561.

Harlow CR, Gems S, Hodges JK, Hearn JP. 1983. The relationship between plasma progesterone and the timing of ovulation and early embryonic development in the marmoset monkey. J Zool. 201:273–282.

Howard B, Chen Y, Zecevic N. 2006. Cortical progenitor cells in the developing human telencephalon. Glia. 53:57–66.

Jacob F. 1977. Evolution and tinkering. Science. 196:1161–1166.

Kosodo Y, Röper K, Haubensak W, Marzesco A-M, Corbeil D, Huttner WB. 2004. Asymmetric distribution of the apical plasma membrane during neurogenic divisions of mammalian neuroepithelial cells. EMBO J. 23:2314–2324.

Kowalczyk T, Pontious A, Englund C, Daza RA, Bedogni F, Hodge R, Attardo A, Bell C, Huttner WB, Hevner RF. 2009. Intermediate neuronal progenitors (basal progenitors) produce pyramidal-projection neurons for all layers of cerebral cortex. Cereb Cortex. 19:2439–2450.

Kriegstein A, Alvarez-Buylla A. 2009. The glial nature of embryonic and adult neural stem cells. Annu Rev Neurosci. 32:149–184.

Kriegstein A, Noctor S, Martinez-Cerdeno V. 2006. Patterns of neural stem and progenitor cell division may underlie evolutionary cortical expansion. Nat Rev Neurosci. 7:883–890.

Kriegstein AR, Götz M. 2003. Radial glia diversity: a matter of cell fate. Glia. 43:37–43.

Lui JH, Hansen DV, Kriegstein AR. 2011. Development and evolution of the human neocortex. Cell. 146:18–36.

Lukaszewicz A, Savatier P, Cortay V, Giroud P, Huissoud C, Berland M, Kennedy H, Dehay C. 2005. G1 phase regulation, area-specific cell cycle control, and cytoarchitectonics in the primate cortex. Neuron. 47:353–364.

Marshall VS, Kalishman J, Thomson JA. 1997. Nonsurgical embryo transfer in the common marmoset monkey. J Med Primatol. 26:241–247.

Paradis E, Claude J, Strimmer K. 2004. APE: analyses of phylogenetics and evolution in R language. Bioinformatics. 20:289–290.

Perelman P, Johnson WE, Roos C, Seuanez HN, Horvath JE, Moreira MA, Kessing B, Pontius J, Roelke M, Rumpler Y, et al. 2011. A molecular phylogeny of living primates. PLoS Genet. 7:e1001342.

Pinto L, Götz M. 2007. Radial glial cell heterogeneity—the source of diverse progeny in the CNS. Prog Neurobiol. 83:2–23.

Preibisch S, Saalfeld S, Tomancak P. 2009. Globally optimal stitching of tiled 3D microscopic image acquisitions. Bioinformatics. 25:1463–1465.

Pulvers JN, Huttner WB. 2009. Brca1 is required for embryonic development of the mouse cerebral cortex to normal size by preventing apoptosis of early neural progenitors. Development. 136:1859–1868.

Rakic P. 1995. A small step for the cell, a giant leap for mankind: a hypothesis of neocortical expansion during evolution. Trends Neurosci. 18:383–388.

Rakic P. 2000. Radial unit hypothesis of neocortical expansion. Novartis Found Symp. 228:30–42; discussion 42–52.

Rakic P. 2009. Evolution of the neocortex: a perspective from developmental biology. Nat Rev Neurosci. 10:724–735.

Reillo I, de Juan Romero C, Garcia-Cabezas MA, Borrell V. 2011. A role for intermediate radial glia in the tangential expansion of the mammalian cerebral cortex. Cereb Cortex. 21:1674–1694.

Sasaki E, Suemizu H, Shimada A, Hanazawa K, Oiwa R, Kamioka M, Tomioka I, Sotomaru Y, Hirakawa R, Eto T, et al. 2009. Generation of transgenic non-human primates with germline transmission. Nature. 459:523–527.

Schluter D, Price T, Mooers AO, Ludwig D. 1997. Likelihood of ancestor states in adaptive radiation. Evolution. 51:1699–1711.

Shitamukai A, Konno D, Matsuzaki F. 2011. Oblique radial glial divisions in the developing mouse neocortex induce self-renewing progenitors outside the germinal zone that resemble primate outer subventricular zone progenitors. J Neurosci. 31:3683–3695.

Smart IH, Dehay C, Giroud P, Berland M, Kennedy H. 2002. Unique morphological features of the proliferative zones and postmitotic compartments of the neural epithelium giving rise to striate and extrastriate cortex in the monkey. Cereb Cortex. 12:37–53.

Stellar E. 1960. The marmoset as a laboratory animal: maintenance, general observations of behavior, and simple learning. J Comp Physiol Psychol. 53:1–10.

Thomson JA, Kalishman J, Hearn JP. 1994. Nonsurgical uterine stage preimplantation embryo collection from the common marmoset. J Med Primatol. 23:333–336.

Wang X, Tsai JW, Lamonica B, Kriegstein AR. 2011. A new subtype of progenitor cell in the mouse embryonic neocortex. Nat Neurosci. 14:555–561.

Zilles K, Armstrong E, Moser KH, Schleicher A, Stephan H. 1989. Gyrification in the cerebral cortex of primates. Brain Behav Evol. 34:143–150.

Zilles K, Armstrong E, Schleicher A, Kretschmann HJ. 1988. The human pattern of gyrification in the cerebral cortex. Anat Embryol. 179:173–179.